Thermal and Material Transport in Nonisothermal Packed Beds

WILLIAM W. SCHERTZ and KENNETH B. BISCHOFF

University of Texas, Austin, Texas

The turbulent transport of mass, energy, and momentum was studied in a 4 in. diameter cylindrical column packed with 0.3 in. diameter stoneware spheres. Helium was used as a tracer material, with air as the mainstream fluid. The concentration of tracer present, the temperature, and the velocity of the gas were measured at several axial and radial increments. These data were analyzed numerically to obtain the radial component of the effective thermal conductivity and the radial component of the mass-dispersion coefficient as functions of radial position. Experimental conditions covered isothermal determinations at room temperature and nonisothermal determinations in which a temperature gradient was established in the radial direction. Significant differences were found between the isothermal and strongly nonisothermal results, primarily for the velocity profiles and thermal conductivities. Correlations were developed for the local values of the parameters.

Heat and mass transfer in packed beds is important in many ways in the chemical industry. Some examples of the use of packed beds are catalytic reactors, chromatographic reactors, ion exchange columns, and contacting towers. The objective of this study was to obtain correlations of the point values of eddy thermal conductivity and mass dispersion coefficients in a nonisothermal system in terms of the physical properties of the packed bed and the fluid flowing through it.

Considerable data has been reported in the literature concerning the prediction of temperatures and concentrations in packed bed reactors (*1* through 9). Much of the effort has utilized the procedure of writing differential mass and energy balances on the reactor, assuming that the packed bed could be treated as a continuum, although alternate methods have also been used (*10, 11*). The resulting differential equations were then simplified by various assumptions to yield equations that could be solved analytically. Results from computations of this type have been useful tools, but have not been completely successful in predicting the performance of actual reactors (*1*). The next level of sophistication was to solve the partial differential equations by numerical methods using high speed computers. This allowed Richardson and Fahien (*12*), for example, to use varying values for the bed properties in calculations of reactor behavior. However, they found that various assumptions utilizing mean value correlations for varying local values gave poor comparison with measured reactor data.

Ideally, one would like the values of the mass and heat transfer dispersion coefficients to be as representative of the real case as possible. In other words, if these parameters are dependent upon temperature level, concentration, position, velocity, etc., knowledge of this dependence is desired so that the most accurate values may be used in design calculations. Yagi and Kunii (*13*) measured effective values of thermal conductivity, and also used values reported by other investigators (*14* through *19*) to develop a correlation that included particle size, mean fluid velocity, and the physical properties of the fluid flowing through the packed bed. Their equation was of the form,

$$\frac{k_e}{k_g} = \frac{k_e^o}{k_g} + (\alpha\beta)\, N_{Re}\, N_{Pr} \tag{1}$$

which correlated an immense quantity of data. Experimental thermal conductivities have been obtained as a function of radial position by Kwong and Smith (*19*); however, they used isothermal velocity data, and did not obtain a correlation of their results.

Mass diffusivity data has been obtained as a function of radial position in a number of experimental studies (*21, 22*). These investigations were all performed in isothermal experiments and the effect of temperature level was not determined.

DEVELOPMENT OF EQUATIONS

A multiple gradient (*23, 24*) mass balance may be written in vector notation as

$$\frac{\partial}{\partial t}\epsilon\,\rho_A + \nabla\cdot\epsilon\,\rho_A\,\mathbf{v} = \nabla\cdot[\epsilon\,\mathbf{D}\,\rho\cdot\nabla\omega_A] + \epsilon\,r_A \tag{2}$$

where all symbols are defined in the nomenclature. Similarly, a multiple gradient energy balance may be written (if the fluid and solid are taken to be at the same temperature),

$$[(1-\epsilon)\,\rho_s\,C_{vs} + \epsilon\,\rho\,C_v]\frac{\partial T}{\partial t} + C_v\,\nabla\cdot(\epsilon\,\rho\,\mathbf{v}T) = \nabla\cdot\mathbf{k}\nabla T + \Delta H_R\,\epsilon\,r_A \tag{3}$$

Substituting

$$\omega_A = \rho_A/\rho, \quad \epsilon\,\rho\,v_r = G_r, \quad \text{and} \quad \epsilon\,\rho\,v_z = G_z,$$

and assuming steady state behavior, angular symmetry, and a nonreacting system, Equation (2) may be written in cylindrical coordinates to give:

$$\frac{1}{r}\frac{\partial}{\partial r}\,r\,G_r\,\omega_A + \frac{\partial}{\partial z}\,G_z\,\omega_A = \frac{1}{r}\frac{\partial}{\partial r}\left[r\,\epsilon\,\rho\,D_r\frac{\partial}{\partial r}\,\omega_A\right] + \frac{\partial}{\partial z}\left[\epsilon\,\rho\,D_z\frac{\partial}{\partial z}\,\omega_A\right] \tag{4}$$

Substituting the equation of continuity,

$$\frac{1}{r}\frac{\partial}{\partial r}\,r\,G_r + \frac{\partial}{\partial z}\,G_z = 0 \tag{5}$$

into Equation (4), and assuming that $G_r << G_z$ (valid for most cases), Equation (6) is obtained

William W. Schertz is with Pratt & Whitney Aircraft, South Windsor, Connecticut. Kenneth B. Bischoff is with the University of Maryland, College Park, Maryland.

$$G_z \frac{\partial}{\partial z} \omega_A = \frac{1}{r} \frac{\partial}{\partial r} \left[r \epsilon \rho D_r \frac{\partial}{\partial r} \omega_A \right] + \frac{\partial}{\partial z} \left[\epsilon \rho D_z \frac{\partial}{\partial z} \omega_A \right] \quad (6)$$

Rearranging Equation (6), similar to Lynn, Corcoran, and Sage (25), and introducing the dimensionless variables $r^* = r/R_o$, $\omega_A{}^* = \omega_A/\bar{\omega}_A$ Equation (7) can be obtained,

$$D_r(r^*) = \frac{R_o^2 \frac{\partial}{\partial z} \int_o^{r^*} \left[r^* G_z(r^*) \omega_A{}^*(r^*) - D_z(r^*) \epsilon(r^*) \rho(r^*, z) \frac{\partial}{\partial z} \omega_A{}^*(r^*) \right] dr^*}{r^* \epsilon \rho \frac{\partial}{\partial r^*} \omega_A{}^*(r^*)} \quad (7)$$

where $\bar{\omega}_A$ is the average concentration of component A in the system and is defined by

$$\bar{\omega}_A = \frac{\int_o^1 2\pi r^* \omega_A(r^*) v_z(r^*) dr^*}{\int_o^1 2\pi r^* v_z(r^*) dr^*} \quad (8)$$

Equation (7) may be further simplified if the value of $D_z(r^*)$ is approximated by

$$D_z(r^*) = C_1 v_z(r^*) \quad (9)$$

which should be sufficiently accurate since mass transfer by dispersion is small compared to mass transfer by convection in the axial direction.

This reduces Equation (7) to

$$D_r(r^*) = \frac{R_o^2 \frac{\partial}{\partial z} \int_o^{r^*} \left[r^* G_z(r^*) \omega_A{}^*(r^*) - C_1 G_z(r^*) \frac{\partial}{\partial z} \omega_A{}^*(r^*) \right] dr^*}{r^* \epsilon \rho \frac{\partial}{\partial r^*} \omega_A{}^*(r^*)} \quad (10)$$

The energy balance [Equation (3)] may be treated in an analogous manner to obtain an expression for the radial component of the thermal conductivity tensor, neglecting the effect of axial thermal conductivity.

$$k_r(r^*) = \frac{R_o^2 \int_o^{r^*} r^* G_z(r^*) C_v \frac{\partial}{\partial z} T \, dr^*}{r^* \frac{\partial}{\partial r^*} T} \quad (11)$$

Equations (10) and (11) were used to evaluate the point values of diffusivity and thermal conductivity with the aid of a numerical computation scheme. Details of the computation methods may be found elsewhere (26).

EXPERIMENTAL WORK

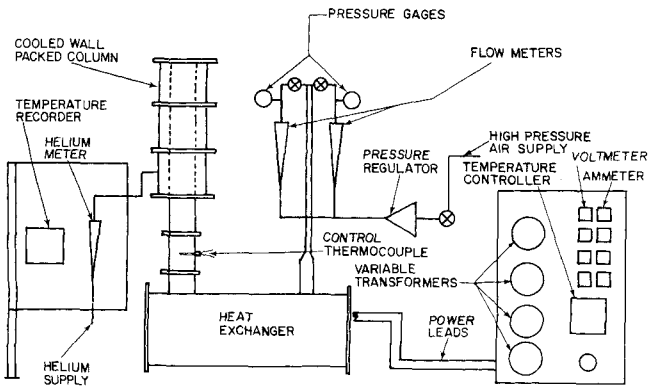

Fig. 1. Equipment schematic.

The flow system used in this investigation is shown schematically in Figure 1. The primary features of the equipment are the following:

1. An air pressure control and metering section.
2. An air heat exchanger and associated power control equipment.
3. A packed bed entrance section.
4. The packed test section.
5. The measurement and analysis equipment.

High pressure air that ranged from 80 to 100 lb./sq.in.gauge was reduced to approximately 20 lb./sq.in.gauge by a pressure regulator and then passed through a bank of flowmeters. A globe valve at the outlet of each flowmeter controlled the flow rate. The pressure at the exit of the flowmeter was maintained at 20 lb./sq.in.gauge so the factory calibration of the flowmeters could be used.

The metered air then passed through the baffled heat exchanger. The 24 heating elements were 1,000 w. electrical heaters, and the power input to the heaters was controlled by a panel of variable transformers. To maintain the outlet temperature at the constant value, four of the electrical heating elements were controlled by a temperature controller. The temperature controller was capable of maintaining the temperature at the exit of the exchanger to within 2°F. of the set point.

The packed bed entrance section was constructed of a 4 in. sch. 40 pipe consisting of an empty 8 in. section followed by a 12 in. section that was packed with 0.305 in. stoneware spheres. The heated air then passed through a packed, water jacketed section that was 13 in. long. This section established the temperature profile in the bed before the start of the test section.

A diagram of the cooled wall column is shown in Figure 2. The annulus through which the cooling water flowed and the helium injection probe are shown. A continuous stream of helium was introduced to the air stream as a tracer material through the ¼ in. O.D. stainless steel tube. The injection probe was centered in the bed.

The test section was a continuation of the cooled wall entrance section. The tip of the injection tube was used as the start of the test section ($Z = 0.0$) and the height of packing in the test section was varied by adding or removing packing to obtain the desired depth. Packing was added by pouring slowly from a container; the bed was not shaken, vibrated, or tapped during the addition of packing. All measurements were made on the gas stream issuing from the top of the packing. This method allowed the measurements to be made without disturbing the packing arrangement.

The duplication of operating conditions when temperature, flow rate, and concentration must be controlled is very difficult; therefore, a probe that can measure temperature and velocity, and collect a sample for concentration analysis simultaneously would be desired. Space limitations and construction difficulties did not permit the construction of one probe that could perform all three functions. Therefore, two separate probes were used and were constructed in a manner that allowed their removal from, or replacement in, the system without changing flow or temperature conditions. Each probe was designed to obtain measurements at several radial positions without being removed from the column, and since the mathematical model used in this study assumed angular symmetry,

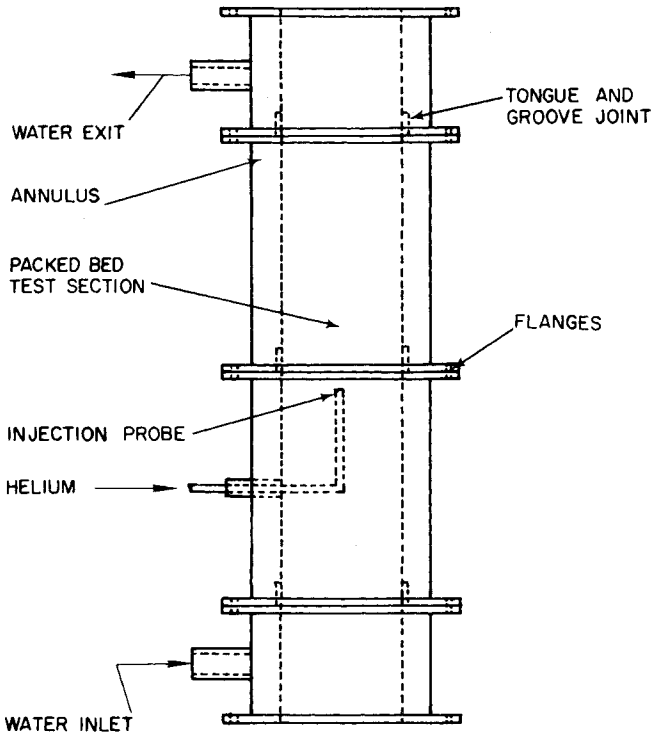

Fig. 2. Water cooled packed column.

the probes were designed to obtain values of velocity, concentration, and temperature that were averaged with respect to the angular coordinate.

Figure 3 is a drawing of the velocity-temperature probe. Velocity measurements were made with a circular hot wire anemometer operated in the constant resistance mode. Additional information on the advantages of constant resistance operation vs. constant current operation may be found elsewhere (*26*). The five 0.008 in. diameter platinum wires were located at radial positions calculated by the equation

$$\frac{r}{R_o} = \left[\frac{(2n-1)}{10}\right]^{1/2}$$

where n is the loop number (1, 2, 3, 4, or 5), and R_o is the radius of the tube. This spacing placed the loops so that they were surrounded by equal areas (*27*); therefore, the total flow rate could be approximately calculated by averaging the individual readings. This spacing arrangement also had the advantage of positioning more anemometer loops near the wall, where previous investigators (*15, 28*) found evidence of a peak in isothermal systems.

The long, large diameter (0.008 in.) wire used for the sensing elements of the anemometer would measure only the average velocity of the gas passing by, and angular variations at each radial position were damped out. The probe was positioned 1 in. above the packing, where the radial components have been shown to damp out (*7*), leaving only the axial component.

Figure 4 is a sketch of the probe that was used to withdraw gas samples from the test section. Samples could be taken at six radial positions without moving the probe assembly. At values of $r/R_o \geq 0.2$, four samples were taken at angular spacings of $\pi/2$ radians through the ⅛ in. thinwall stainless steel sampling tubes. These samples were mixed in the inner cylinder and withdrawn as a single averaged sample. At the center of the bed ($r/R_o = 0$) only one sample tube was used, as shown in Figure 4. The central tube of the probe was attached to a piston, which was sealed to the inner wall of the outer tube by Teflon O-rings. Moving the central tube vertically aligned the ports in the piston with the ⅛ in. sampling tubes for sampling at values of $r/R_o \geq 0.2$. When the piston was forced fully downward, the lower Teflon O-ring did not make contact with the expanded cylinder wall, and thus allowed gas from the center sampling tube to flow into the central tube for removal and analysis. The device gave only angular blended samples and angular variations were not measured; this should be sufficient for design purposes, however.

The concentration of helium tracer gas was analysed with a thermal conductivity cell with air as a reference gas. A complete description of the flow circuits operation is given elsewhere (*26*). The output of the thermal conductivity cell was recorded on a recorder that was sensitive to 0.2 mv. signals. This corresponded to 0.01% He for a 3 hr. period.

RESULTS

Velocity Profile Results

The hot wire anemometer was found to be a relatively rugged device for the measurement of the velocity of hot gases exiting from the packed bed. The calibration of the device was very time consuming because of the large number of data points needed. However, after the calibration was completed, the probe did not change properties significantly over a two-month period of use. Velocity measurements with the probe were found to be within 8% of the actual velocity when the axial velocity was greater than 1 ft./sec. The sensitivity of the probe decreased rapidly for velocities below 1 ft./sec.

The smoothed velocity profiles for the various cases studied are shown in Figures 5 to 9. These velocity profiles demonstrate a rise in velocity near the wall of the

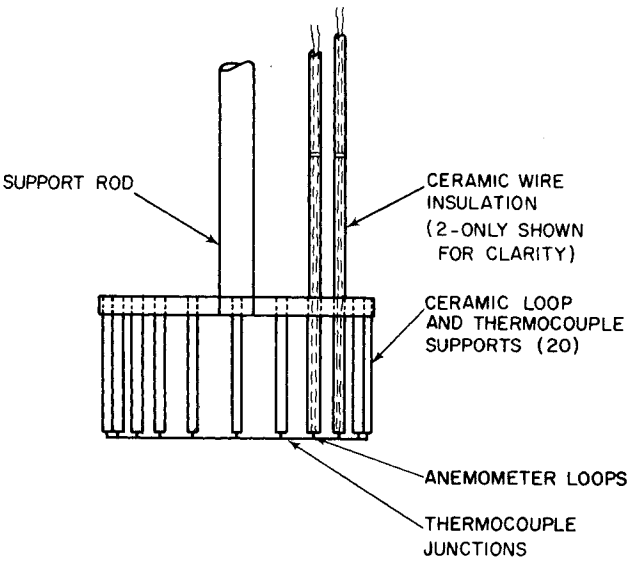

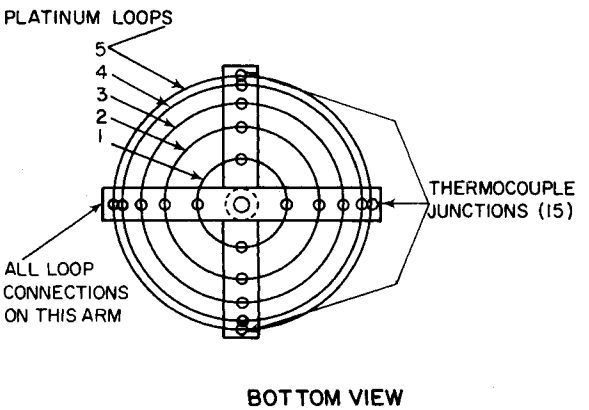

Fig. 3. Temperature-velocity probe.

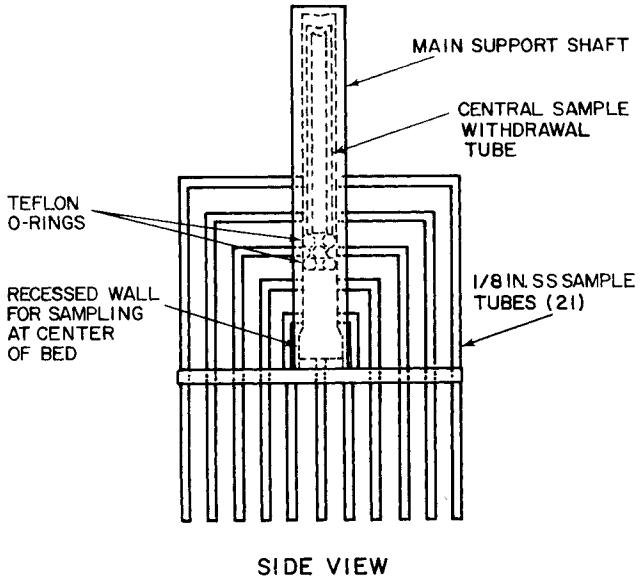

Fig. 4. Concentration probe.

packed bed, as also found by previous investigators (*15, 22, 28, 29*) for isothermal measurements. It should be noted that the effect is much more pronounced when a temperature gradient is present and the center of the bed is hotter than the edge. This amplification of the wall channeling was anticipated because of the increase in the viscosity of gases with temperature.

For design purposes, a correlation between the velocity and the physical properties of the system is desirable. A hydraulic radius (r_H) can be defined as

$$r_H = \frac{\epsilon\, d_p}{6(1-\epsilon)} \qquad (12)$$

for radial positions less than $r/Ro = 0.9$, and by a geometric calculation of (area available for flow)/(wetted perimeter) for $0.9 \leq r/Ro \leq 1.0$ (*26*). Calculated values of hydraulic radius using data from Benenati and Brosilow (*30*) and Roblee, et al. (*31*) are shown in Figure 10. The hydraulic radius and viscosity of the gas (calculated from the temperature) were used in a correlation of the velocity profiles as shown in Figure 11, which includes the data from all nine cases, covering isothermal and nonisothermal operating conditions. When the centerline temperature was the highest, the velocity in the center of the bed was very low and the flow became laminar, even though the total flow rate through the bed was high. This transition from turbulent flow to laminar flow is evident as a break in the curve in Figure 11, in which $Gd_p/G_o r_H$ is plotted as a function of the viscosity difference ratio $\mu - \mu_o/\mu_o$. G is the mass velocity of the gas leaving the packing, G_o is the superficial mass velocity passing through the empty column, r_H is the hydraulic radius, μ is the viscosity of the gas, and μ_o is the gas viscosity at room temperature.

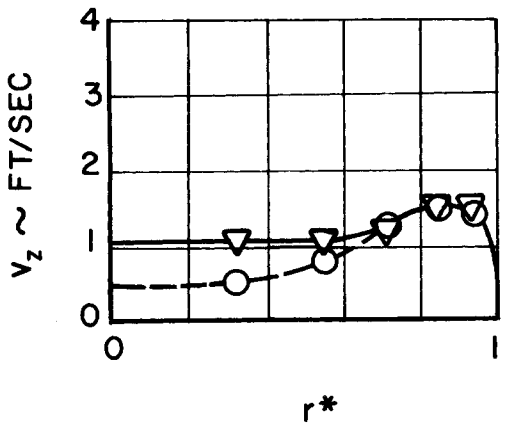

Fig. 5. Velocity vs. radial position, 5 std. cu. ft./min.
Isothermal - - - -
Nonisothermal ———
Centerline at 231°F.

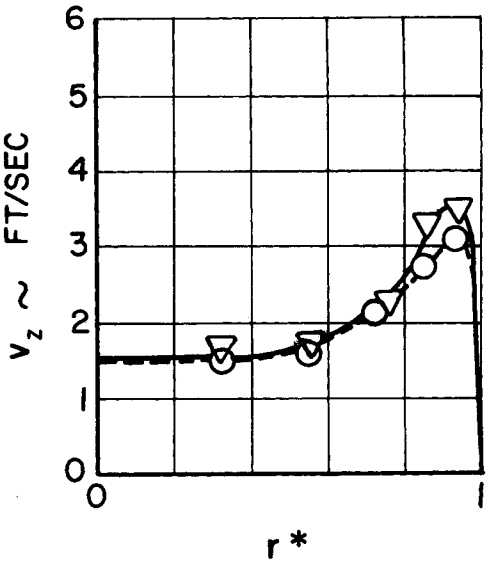

Fig. 6. Velocity vs. radial position, 10 std. cu. ft./min.
Isothermal - - - -
Nonisothermal ———
Centerline at 325°F.

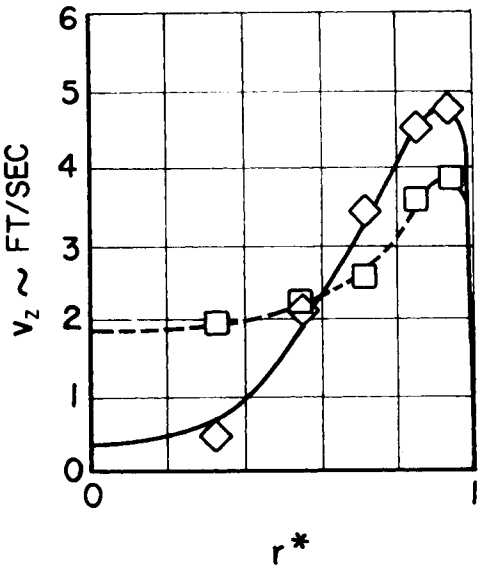

Fig. 7. Velocity vs. radial position, 13 std. cu. ft./min.
Isothermal - - - -
Nonisothermal ———
Centerline at 342°F.

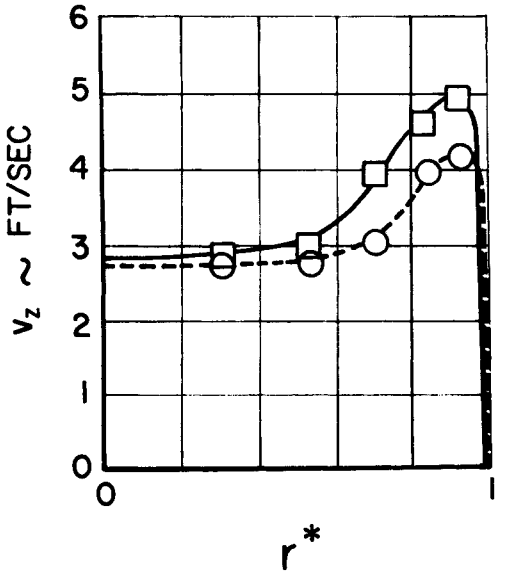

Fig. 8. Velocity vs. radial position, 15 std. cu. ft./min.
Isothermal - - - -
Nonisothermal ———
Centerline at 238°F.

Concentration and Mass Diffusivity Results

Because of the large amount of experimental concentration data (*26*) that was needed for this study, it is impractical to show the concentration profiles for every case. Therefore only the curves for a volumetric flow rate of 5 std.cu.ft./min. are shown as smoothed data in Figure 12. The point values of mass diffusivity [$D_r\ (r^*)$] were calculated from the concentration, velocity and temperature data using Equation (10). An analysis of the data and computational scheme (see Appendix) showed that the calculation of $D_r\ (r^*)$ should be performed only for $4 \leq z \leq 8$ in.

The results of the computation of radial mass diffusivities are shown in Figures 13 and 14. These curves show the dependence of mass diffusivity on radial position, and are the result of averaging the curves obtained for several values of Z. There was no distinct dependence upon axial position (*26*).

The diffusivity curves obtained for all of the nine different cases studied demonstrated the effect of increasing velocity near the edge of the tube. No values extremely close to the wall could be calculated; however, the radial diffusivity coefficient must go to the value of the molecular diffusion coefficient at the wall. The broken line portion of Figures 13 and 14 is the extrapolation of the diffusivity to the value of the molecular diffusion coefficient. The shape of the $D_r\ (r^*)$ vs. r^* curves suggests that a dependence of $D_r\ (r^*)$ upon the interstitial velocity may exist. To test this hypothesis the point values of the Peclet Number were calculated. The results gave highly scattered points with a mean value of

$$d_p\, v_z\ (r^*)/D_r\ (r^*) = 8$$

The Peclet Number based on the interstitial velocity was more or less constant over the radial dimension, and there was no evidence of an effect of temperature level or temperature gradients on the values. The data were very scattered and it is not felt that much confidence could be placed on any other trends.

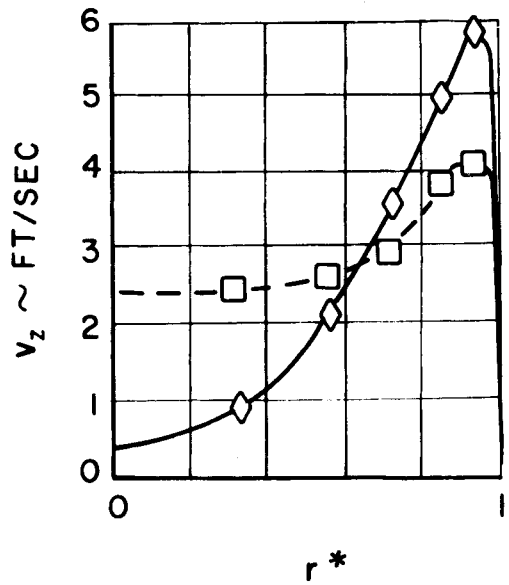

Fig. 9. Velocity vs. radial position, 15 std. cu. ft./min.
Isothermal - - - -
Nonisothermal ———
Centerline at 360°F.

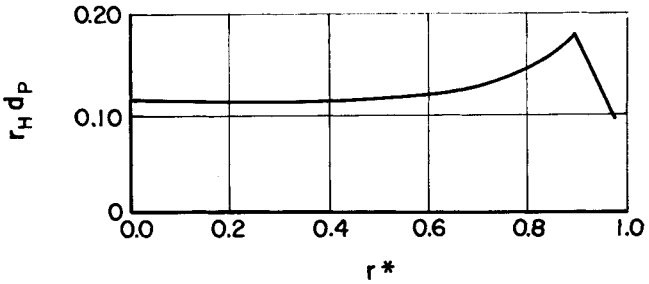

Fig. 10. Hydraulic radius vs. radial position.

Temperature Data and Thermal Conductivity Results

A temperature profile obtained is presented graphically in Figure 15. The lines represent the smoothing function used to help minimize the effect of experimental error. The smoothed temperature data were used to calculate radial thermal conductivities, using Equation (11). The conductivities were then correlated by an equation similar to that to Yagi and Kunii (*13*),

$$\frac{k_r\ (r^*)}{k_g} = \frac{k^\circ_e}{k_g} + C_2 N_{Re} N_{Pr} \qquad (13)$$

where N_{Re} is the local interstitial Reynolds number $d_p v_z\ (r)\ \rho/\mu$, N_{Pr} is the Prandtl number $C_p\ \mu/k_g$, C_2 is an empirical constant, and k_g is the thermal conductivity of the gas. The results of the correlation are shown in Figure 16, and a comparison is made between these results and the results of Yagi and Kunii for similar systems. Excellent agreement between the two results are obtained; however, it should be remembered that Yagi and Kunii's correlation is based upon an overall Reynolds number,

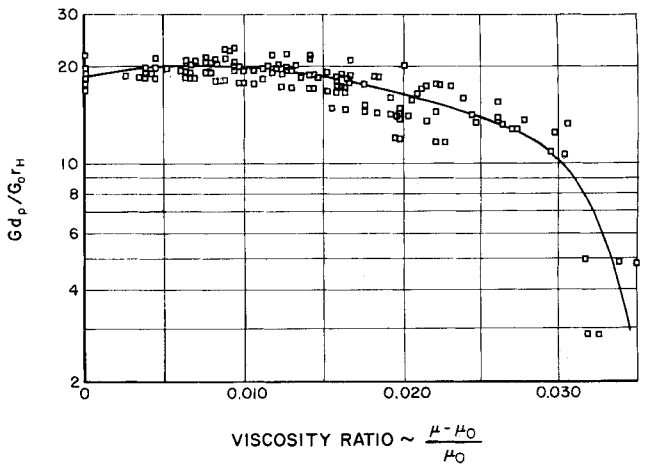

Fig. 11. Velocity correlation.

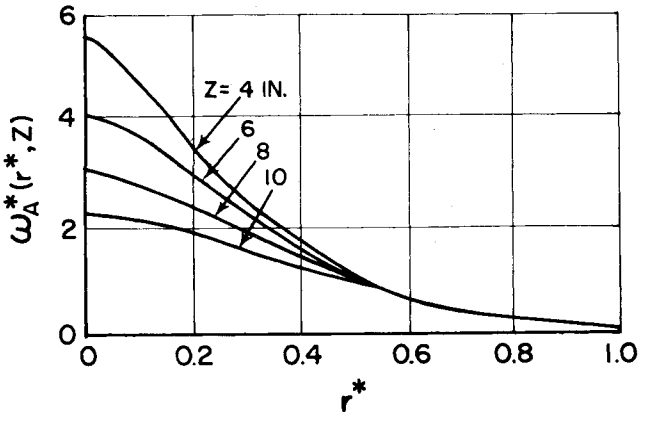

Fig. 12*a*. Concentration vs. radial position, 5 std. cu. ft./min.

and an overall effective thermal conductivity (k_e). The results of this work indicate that if the interstitial Reynolds number is used, the point values of thermal conductivity may be obtained, and the results of Yagi and Kunii's correlations for effective conductivities may hopefully be utilized for other cases. This correlation exemplifies the need for knowledge of point values of the axial velocity in packed beds since it seems to be the most critical variable. The correlation for velocity presented here is a beginning, but more experimental data covering a variety of packing sizes with different fluids and broader temperature ranges needs to be obtained for a complete design basis.

ACKNOWLEDGMENT

The support of the National Science Foundation through grant NSF GP-865 is gratefully acknowledged.

NOTATION

C_{VS} = heat capacity of solid, $M/(LT^2\theta)$
C_V = heat capacity of gas phase, $M/(LT^2\theta)$
$\mathbf{D}$ = mass diffusivity tensor, L^2/T
D_r = radial component of mass diffusivity tensor, L^2/T
D_z = axial component of mass diffusivity tensor, L^2/T
d_p = diameter of particle, L
d_t = diameter of tube, L
G_o = superficial mass average velocity based on tube area, $M/(L^2T)$

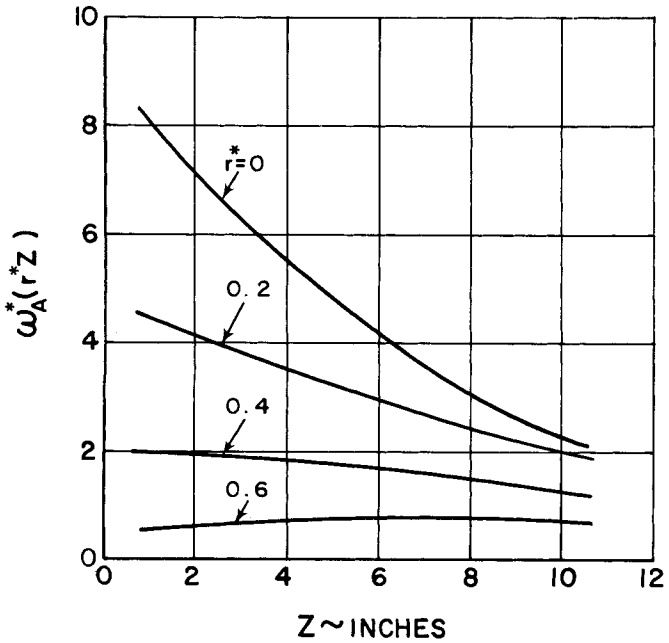

Fig. 12*b*. Concentration vs. axial position, 5 std. cu. ft./min.

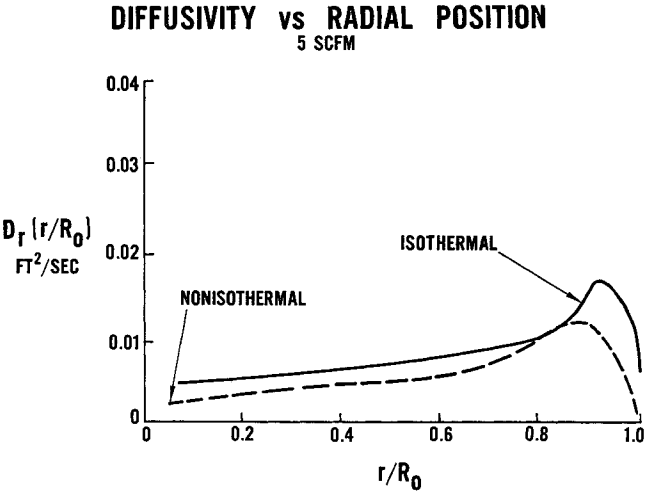

Fig. 13. Dispersion coefficient [$D_r(r^*)$] vs. radial position, 5 std. cu. ft./min.

G_r = radial component of superficial mass average velocity, $M/(L^2T)$
G_z = axial component of superficial mass average velocity, $M/(L^2T)$
$\mathbf{k}$ = thermal conductivity tensor, $ML/(T^2\theta)$
$k_{r,z}$ = radial or axial component of k, $ML/(T^2\theta)$
k_e = effective radial thermal conductivity assumed constant over entire radius, $ML/(T^2\theta)$
k_g = thermal conductivity of the gas phase, $ML/(T^2\theta)$
k°_e = effective radial thermal conductivity at zero flow rate, $ML/(T^2\theta)$
N_{pe} = Peclet number, vd_p/D_r
N_{Pr} = Prandtl number, $C_p\mu/k_g$
N_{Re} = Reynolds number, $d_p v_z \rho/\mu$, or $d_p G_o/\mu$ (not equivalent)
R_o = radius of tube = $d_t/2$, L
r = radial position, L
r_H = hydraulic radius, L
r^* = dimensionless radial position = r/R_o
t = time or temperature (°F. or °C.), T, θ
T = temperature °K. or °R.
$\mathbf{v}$ = velocity in interstices, L/T^2
$v_{z,y,z}$ = x, y, or z component of $\mathbf{v}$, L/T^2
x, y, z = coordinate labels, L

Greek Symbols

ϵ = void fraction in packed bed
μ = eddy viscosity tensor, M/LT
μ = viscosity of gas, M/LT
μ_o = viscosity of gas at standard conditions, M/LT

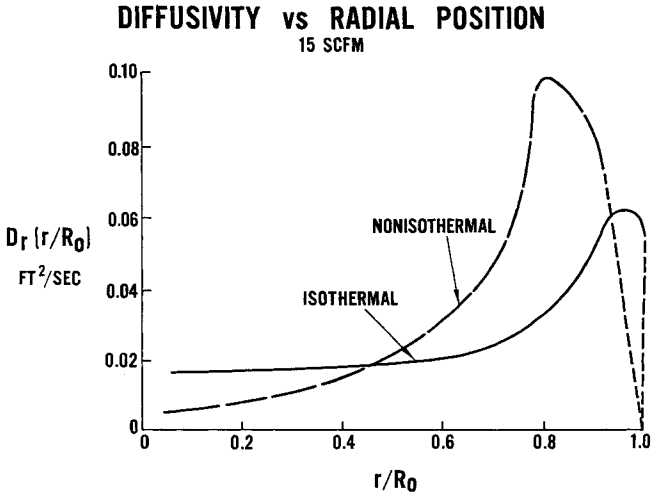

Fig. 14. Dispersion coefficient [$D_r(r^*)$] vs. radial position, 15 std. cu. ft./min.

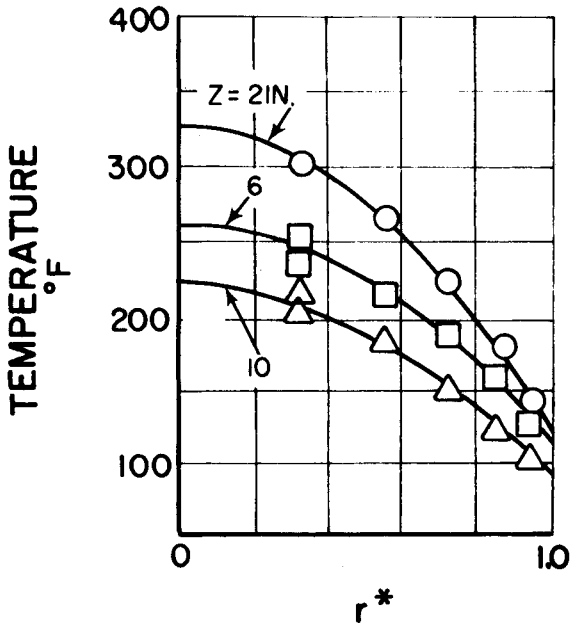

Fig. 15. Radial temperature profiles, 10 std. cu. ft./min. Centerline at 325°F.

ρ_A = concentration of A in gas phase, M/L^3
ρ = density of gas phase, M/L^3
ρ_s = density of solid phase, M/L^3
ω_A = mass fraction of A in gas phase
$\overline{\omega}_A$ = average concentration of A (mass fraction) at a particular value of z
∇ = del operator
θ = dimension of temperature

LITERATURE CITED

1. Baron, T., *Chem. Eng. Progr.*, **48**, 118 (1952).
2. Mickley, H. S., and R. W. M. Letts, *Can. J. Chem. Eng.*, **41**, 273 (1963).
3. Carberry, J. J., and M. M. Wendel, *AIChE J.*, **9**, 129 (1963).
4. Beek, J., *Adv. Chem. Eng.*, **3**, 204 (1962).
5. Bischoff, K. B., *Ind. Eng. Chem.*, **58**, No. 11, 18 (1967).
6. Carberry, J. J., *Chem. Process Eng.*, **44**, 306 (1963).
7. Levenspiel, O., and K. B. Bischoff, *Adv. Chem. Eng.*, **4**, 95 (1963).
8. Froment, G. F., *Ind. Eng. Chem.*, **59**, No. 2, 18 (1967).
9. Wilhelm, R. H., *Pure Appl. Chem.*, **5**, 403 (1962).
10. Deans, H. A. and L. Lapidus, *AIChE J.*, **6**, 656 (1960).
11. McGuire, M. L., and L. Lapidus, *ibid.*, **11**, 85 (1965).
12. Richardson, R. C., and R. W. Fahien, paper presented at AIChE meeting, Houston, Texas (Dec., 1963).
13. Yagi, S., D. Kunii, and N. Wakao, paper presented at the Intern. Heat Transfer Conf., Boulder, Colorado (1960).
14. Argo, W. B., and J. M. Smith, *Chem. Eng. Progr.*, **49**, 443 (1953).
15. Morales, M., C. W. Spinn, and J. M. Smith, *Ind. Eng. Chem.*, **43**, 225 (1951).
16. Schotte, W., *AIChE J.*, **6**, 63 (1960).
17. Schuler, R. W., V. P. Stallings, and J. M. Smith, *Chem. Eng. Progr. Symposium Ser.*, No. 4, **48**, 19 (1952).
18. Yagi, S., and N. Wakao, *AIChE J.*, **5**, 79 (1959).
19. Kwong, S. S., and J. M. Smith, *Ind. Eng. Chem.*, **49**, 894 (1957).
20. Bernard, R. A., and R. H. Wilhelm, *Chem. Eng. Progr.*, **46**, 223 (1950).
21. Frandolig, J. E., U.S.A.E.C. Rept. No. ISC-908 (1957).
22. Fahien, R. W., and J. M. Smith, *AIChE J.*, **1**, 28 (1955).
23. Himmelblau, D. M., and K. B. Bischoff, "Process Analysis and Simulation," John Wiley, New York (1967).
24. Bird, R. B., W. E. Stewart, and E. N. Lightfoot, "Transport Phenomena," John Wiley, New York (1960).
25. Lynn, S., W. H. Corcoran, and B. H. Sage, *AIChE J.*, **3**, 11 (1957).
26. Schertz, W. W., Ph.D. thesis, Univ. Texas, Austin (1967).
27. Perry, J. H., ed., "Chemical Engineers Handbook," 3 Ed., McGraw-Hill, New York (1950).
28. Schwartz, C. E., and J. M. Smith, *Ind. Eng. Chem.*, **45**, 1209 (1953).
29. Dorweiler, V. P., and R. W. Fahien, *AIChE J.*, **5**, 139 (1959).
30. Benenati, R. F., and C. B. Brosilow, *ibid.*, **8**, 359 (1962).
31. Roblee, L. H. S., R. M. Baird, and J. W. Tierney, *ibid.*, **4**, 460 (1958).

Manuscript received October 3, 1967; revision received April 15, 1968; paper accepted April 17, 1968. Paper presented at AIChE Salt Lake City meeting.

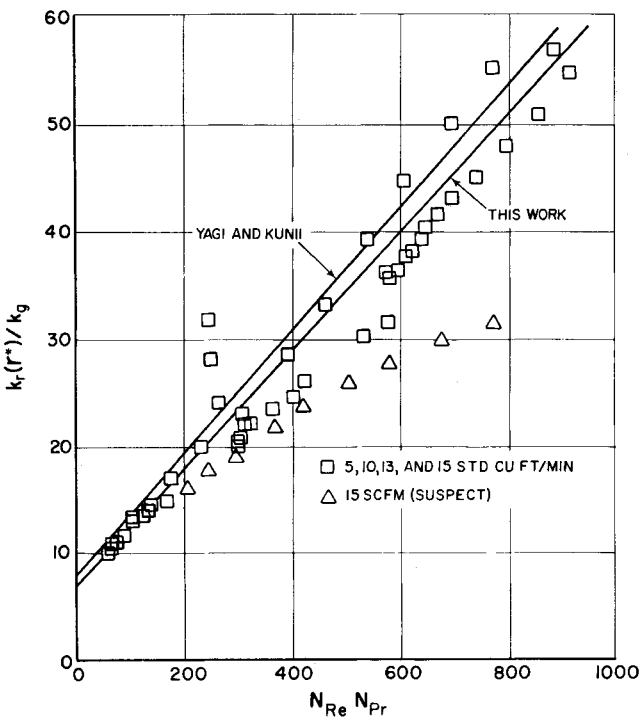

Fig. 16. Thermal conductivity correlation.

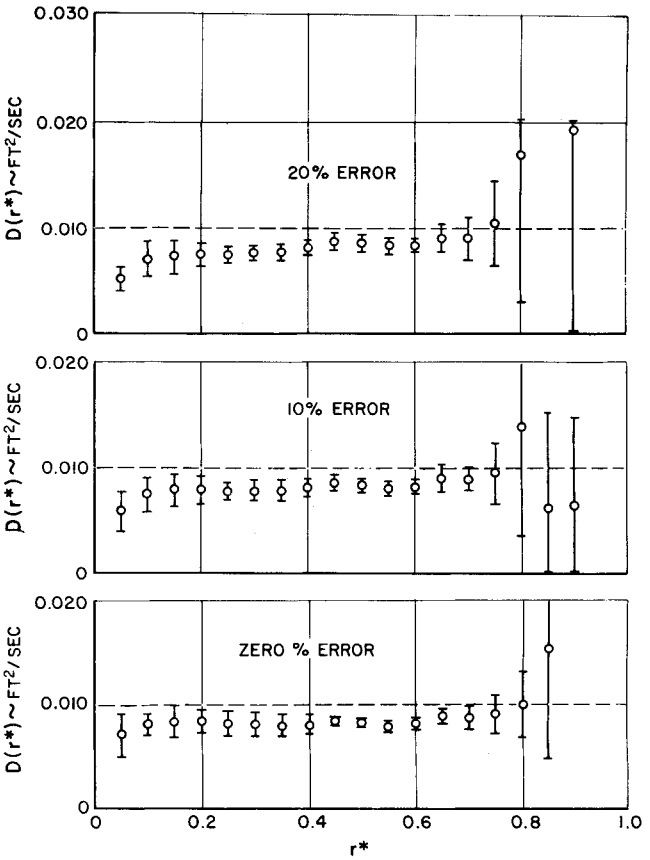

Fig. 17. The effect of random error on the calculated values of $D_r(r^*)$.

APPENDIX: ERROR ANALYSIS

To evaluate the amount of the error induced in the diffusivity values by the multiple differentiations and integrations that were performed numerically on the experimental data, the computational scheme was used to analyze some artificial data with a known constant diffusivity. The data were generated by solving the special case of Equation (6) in cylindrical coordinates in which v_z, D, and ρ were all constant. Equation (6) then can be reduced to

$$\frac{\partial}{\partial z}\rho_A = \frac{1}{\alpha}\left[\frac{1}{r}\frac{\partial}{\partial r}r\frac{\partial \rho_A}{\partial r} + \frac{\partial^2}{\partial z^2}\rho_A\right] \tag{A1}$$

where $\alpha = v_{z/D}$

The appropriate boundary conditions are

$$\left.\frac{\partial \rho_A}{\partial r}\right|_{r=1} = 0 = \left.\frac{\partial}{\partial r}\rho_A\right|_{r=1} \tag{A2}$$

$$\lim_{z\to\infty}[\rho_A] = \rho_{A\text{mean}}$$

The set of Equations (A1) and (A2) has the solution as given by Bernard and Wilhelm (*20*),

$$\rho_A(r, z) = \rho_{A\text{mean}} + \sum_{n=0}^{\infty}\left[\frac{\alpha_e[\alpha - (\alpha^2 + 4\beta_n^2)^{1/2}]^{z/2}}{J_o^2(\beta_n R_o)\,(\alpha^2 + 4\beta_n^2)^{1/2}}\right] J_o(\beta_n r) \tag{A3}$$

where the β_n are the roots of

$$J_1(\beta_n R_o) = 0 \tag{A4}$$

Equation (A3) was used to generate concentration profiles for various values of $\alpha = v_{z/D}$. This data was then analyzed by the numerical scheme that was devised for the evaluation of Equation (10) and the resulting values of $D_r(r^*)$ compared with the theoretical value that had been used to generate the data. The entire process was repeated twice with random error of 0 to 10% and 0 to 20% being added to the concentration values. This was done to simulate the presence of experimental error in the actual data. The results of these computations are shown in Figure 17 for one particular value of α, and the deviation at each radial position is indicated. These results demonstrate that the numerical procedure has the greatest deviation at the center of the bed and near the edges. This is expected since the denominator of Equation (10) approaches zero in these regions.

As can be seen from Figure 17, the addition of random error does not cause rapid generation of instabilities in the computed results, and up to 20% error in the concentration data can be handled by the program.

The Flow Characteristics of Swirl (Centrifugal) Spray Pressure Nozzles with Low Viscosity Liquids

NORMAN DOMBROWSKI and DAVID HASSON

Imperial College, London, England

A study has been made of the mechanics of flow of low viscosity liquids through swirl spray nozzles. Discharge coefficients and spray angles have been measured for a series of nozzles designed to systematically determine dimensional effects not predicted by frictionless theory, in particular the effect of the ratios of swirl chamber diameter to orifice diameter and of orifice length to orifice diameter. It was found that a unique relationship exists between discharge coefficient and spray angle dependent only upon the value of the orifice length/diameter ratio. This result has been explained on the basis of an ideal flow theory extended to take into account the frictional decay of the vortex motion. A general expression has been derived which permits correlation of the flow characteristics of nozzles covering a wide range of designs.

Swirl (or centrifugal) spray pressure nozzles are probably the commonest type of atomizer to be found in industry and numerous fundamental studies have been carried out in order to relate the spray angle and discharge coefficient to the nozzle dimensions. However, except under very limited conditions none of the present theories is sufficiently reliable and for most applications design methods follow empirical lines.

Published data is inadequate to allow accurate assessments to be made of the effect of nozzle dimensions on the flow characteristics, information on the spray angle being particularly meager. Further data have therefore been collected using a series of about 80 accurately manufactured nozzles. A theory is presented which extends the range of existing design methods for low viscosity liquids and allows the correlation of the flow characteristics of a range of nozzle designs.

Norman Dombrowski is at The University, Leeds, England. David Hasson is at The Technion, Haifa, Israel.